HHS Public Access

Author manuscript

Dev Biol. Author manuscript; available in PMC 2017 August 15.

Published in final edited form as:

Dev Biol. 2016 August 15; 416(2): 324–337. doi:10.1016/j.ydbio.2016.06.025.

Loss of *laminin alpha 1* results in multiple structural defects and divergent effects on adhesion during vertebrate optic cup morphogenesis

Chase D. Bryan[1], **Chi-Bin Chien**[2,*], and **Kristen M. Kwan**[1]

[1]Department of Human Genetics, University of Utah, Salt Lake City, UT 84112

[2]Department of Neurobiology and Anatomy, University of Utah, Salt Lake City, UT 84112

Abstract

The vertebrate eye forms via a complex set of morphogenetic events. The optic vesicle evaginates and undergoes transformative shape changes to form the optic cup, in which neural retina and retinal pigmented epithelium enwrap the lens. It has long been known that a complex, glycoprotein-rich extracellular matrix layer surrounds the developing optic cup throughout the process, yet the functions of the matrix and its specific molecular components have remained unclear. Previous work established a role for laminin extracellular matrix in particular steps of eye development, including optic vesicle evagination, lens differentiation, and retinal ganglion cell polarization, yet it is unknown what role laminin might play in the early process of optic cup formation subsequent to the initial step of optic vesicle evagination. Here, we use the zebrafish *lama1* mutant (*lama1*^{UW1}) to determine the function of laminin during optic cup morphogenesis. Using live imaging, we find, surprisingly, that loss of laminin leads to divergent effects on focal adhesion assembly in a spatiotemporally-specific manner, and that laminin is required for multiple steps of optic cup morphogenesis, including optic stalk constriction, invagination, and formation of a spherical lens. Laminin is not required for single cell behaviors and changes in cell shape. Rather, in *lama1*^{UW1} mutants, loss of epithelial polarity and altered adhesion lead to defective tissue architecture and formation of a disorganized retina. These results demonstrate that the laminin extracellular matrix plays multiple critical roles regulating adhesion and polarity to establish and maintain tissue structure during optic cup morphogenesis.

Keywords

eye morphogenesis; laminin; adhesion; cell polarity; retina; lens

Corresponding author: Kristen M. Kwan, Department of Human Genetics, EIHG 5100, University of Utah Medical Center, 15 North 2030 East, Salt Lake City, UT 84112, phone: 801-585-7541, fax: 801-581-7796, kristen.kwan@genetics.utah.edu.

*Deceased

Author Contributions

C.D.B., C.-B.C., and K.M.K. conceived of the experiments and developed the concepts. C.D.B. and K.M.K. performed experiments and data analysis, and C.D.B. and K.M.K. prepared and edited the manuscript prior to submission.

Introduction

In vertebrates, the eye initially forms as an outpocketing of tissue from the prospective brain neuroepithelium. The newly formed optic vesicle then undergoes a series of complex cell and tissue movements - including elongation, rotation, and invagination - to form the optic cup, which is comprised of neural retina and retinal pigmented epithelium enwrapping the lens. The cellular processes - movements, divisions, tissue-tissue interactions, and shape changes - underlying these morphogenetic events are beginning to be elucidated via a combination of live imaging and quantitative histology (Chow and Lang, 2001; England et al., 2006; Fuhrmann, 2010; Heermann et al., 2015; Ivanovitch et al., 2013; Kwan et al., 2012; Martinez-Morales and Wittbrodt, 2009; Picker et al., 2009; Rembold et al., 2006; Yang, 2004). But while the cellular processes comprising optic cup formation are being described, we lack a comprehensive understanding of the molecular pathways controlling these critical movements.

A compelling molecular candidate for regulating optic cup morphogenesis is the extracellular matrix component laminin. It has been known for decades that in all vertebrates, a glycoprotein-rich layer surrounds the developing optic cup and lens, and that laminin is a significant component of this meshwork (Hendrix and Zwaan, 1975; Hilfer and Randolph, 1993; Kurkinen et al., 1979; McAvoy, 1981; Parmigiani and McAvoy, 1984; Peterson et al., 1995; Svoboda and O'Shea, 1987; Tuckett and Morriss-Kay, 1986; Wakely, 1977; Webster et al., 1983, 1984). Laminin proteins form heterotrimers comprised of α, β, and γ chains. There are multiple forms of each chain in vertebrates, although the laminin-111 species (the heterotrimer of lama1 (laminin-α 1), lamb1 (laminin-β1), and lamc1 (laminin-γ1)) is considered to be the predominant isoform during early development (Colognato and Yurchenco, 2000; Miner and Yurchenco, 2004). In zebrafish, multiple laminin chains are expressed during the period of optic cup morphogenesis, but their functional roles during this process are largely unexplored.

Functional roles for laminin have been elucidated primarily using *in vitro* cell culture systems. As a part of the extracellular matrix, laminin serves as an adhesive substrate, yet how it interacts *in vivo* with other ECM components to modulate adhesion and focal adhesion assembly is poorly understood. It is known that laminin impacts cell survival: loss of attachment can lead to anoikis, a specific form of programmed cell death (Frisch and Francis, 1994; Juliano et al., 2004). Laminin can also regulate cell migration, in particular lamellipodial protrusions (Adams and Watt, 1993; Daley and Yamada, 2013). Finally, laminin is often critical for establishing and maintaining epithelial cell polarity, by serving as an extrinsic cue to specify the basal surface (Martin-Belmonte and Mostov, 2008). A role for laminin in optic cup formation could affect any – or all – of these processes: it is unclear which might be crucial for the actual morphogenetic process.

In zebrafish, mutant analysis has revealed many roles for lama1, including in development of notochord, muscle, and brain structure, neurogenesis, neuronal migration, and axon guidance (Biehlmaier et al., 2007; Grant and Moens, 2010; Jiang et al., 1996; Karlstrom et al., 1996; Parsons et al., 2002; Paulus and Halloran, 2006; Pollard et al., 2006; Schier et al., 1996; Sittaramane et al., 2009; Sztal et al., 2012; Wolman et al., 2008). In the visual system,

previous work has defined roles for different laminin chains in various steps of eye development, with most studies focusing on later stages after optic cup formation. Analysis of *lamb1* and *lamc1* mutants revealed coloboma, structural defects in the eye indicating failure of some aspect of choroid fissure development (Lee and Gross, 2007). *lama1* mutants display lens degeneration, as well as defects in development of the ocular anterior segment, including cornea and iris (Pathania et al., 2014; Semina et al., 2006; Zinkevich et al., 2006). Less is known, however, about earlier stages of eye development, specifically optic cup formation. Detailed analysis of the initiating event, optic vesicle evagination, indicates that laminin (specifically, the *lamc1* mutant was examined) plays a critical role in organizing, coordinating, and delimiting the polarized elongation of retinal progenitors just as the optic vesicle emerges (Ivanovitch et al., 2013). By the end of optic cup formation, *lamb1* and *lamc1* mutants appear to exhibit a “protruding lens” phenotype (Parsons et al., 2002), suggesting some defect in the process of optic cup morphogenesis, possibly invagination. However, the phenotype has not been studied in detail, and underlying cellular defects during optic cup formation have not been identified.

Taken together, these data suggest critical roles for laminin extracellular matrix proteins during eye development, yet much remains to be determined. What role does laminin play throughout optic cup morphogenesis? Are there specific tissue morphogenetic events that are dependent upon laminin? How does laminin regulate focal adhesion assembly, specifically during these morphogenetic events, and what other functions might laminin carry out? To address these questions, we are using the zebrafish mutant *bashful*^{UW1} (also called *lama1*^{UW1}), in which the *laminin alpha 1* (*lama1*) gene is disrupted (Paulus and Halloran, 2006; Semina et al., 2006). Using 4D timelapse imaging and visualization, we determine how loss of *lama1* affects optic cup morphogenesis beyond evagination. We examine focal adhesion assembly during optic cup formation, determine how this is disrupted by loss of *lama1*, and then investigate how loss of *lama1* affects several aspects of tissue morphogenesis, including cell survival, migration, shape changes, and polarity. Our data suggest that the laminin extracellular matrix is required for multiple specific morphogenetic events, acting through establishment of cell polarity and spatiotemporally-specific regulation of focal adhesion assembly.

Material and Methods

Zebrafish

Embryos from *lama1*^{UW1} heterozygous incrosses were raised at 28.5–30°C and staged according to time post fertilization and morphology (Kimmel et al., 1995). For all experiments, control embryos consisted of *lama1*^{UW1} wild type and heterozygous carrier siblings.

RNA synthesis and injections

Capped RNA was synthesized using pCS2 templates (pCS2-EGFP-CAAX, pCS2FA-H2A.F/Z-mCherry, pCS2FA-mCherry-CAAX, pCS2-EGFP-vinculin, pCS2-pard3-GFP), the mMessage mMachine SP6 kit (Ambion), purified (Qiagen RNeasy Mini Kit) and ethanol precipitated. 300–500 pg RNA (EGFP-CAAX, H2A.F/Z-mCherry, pard3-GFP) was injected

into the cell of 1-cell stage embryos. For analysis of focal adhesion assembly, EGFP-vinculin and mCherry-CAAX (250 pg RNA each) were co-injected into the cell of 1-cell stage embryos.

Antibody staining

Embryos were fixed at the appropriate stage in 4% paraformaldehyde, permeabilized in TBST (TBS+0.1% Triton X-100), and blocked in TBST+2% BSA. Anti-laminin antibody (Sigma #L9393) was diluted 1:100, anti-vinculin antibody (Sigma #V4505) was diluted 1:100, anti-activated caspase-3 antibody (BD Pharmingen #559565) was diluted 1:200, anti-aPKC (PKC ζ (C-20) Santa Cruz Biotechnology #sc-216) was diluted 1:100, anti-fibronectin antibody (Sigma #F3648) was diluted 1:100. Alexa Fluor 488 goat anti-rabbit secondary (Life Technologies, A-11008) or Alexa Fluor 488 goat anti-mouse secondary (Life Technologies, A-11001) was coincubated with 1 μM TOPRO-3 iodide (Life Technologies, T3605). Embryos were cleared in 70% glycerol for imaging.

Imaging

For timelapse imaging, embryos (12 hpf) were dechorionated, embedded in 1.6% low melting point agarose (in E2+gentamycin) in DeltaT dishes (Bioptechs, #0420041500C). E2+gentamycin was overlaid, and the dish covered to prevent evaporation. Images were acquired using an Olympus FV1000 or Zeiss LSM710 laser scanning confocal microscope. 4-dimensional datasets were acquired: all datasets except for EGFP-vinculin imaging were acquired with the following parameters: 36 z-sections, 3.52 μm z-step, 40X water-immersion objective (1.15 NA). EGFP-vinculin 4-dimensional datasets (Fig. 3) were acquired with the following parameters: 63 z-sections, 2.1 μm z-step, 40X water-immersion objective (1.2 NA). For in toto eye imaging, time between z-stacks was 3.43 minutes (Fig. 1), 3.5 minutes (Fig. 3), 4.22 minutes and 4 minutes (Fig. 5 control and mutant, respectively), and 4.5 minutes (Fig. 6).

For Kaede photoconversion, Olympus Fluoview or Zeiss Zen software was used to expose a rectangular R.O.I. to 405 nm light for 15–20 seconds. Efficiency of photoconversion was assayed by loss of green and gain of red fluorescence in the R.O.I.

For all timelapse imaging experiments, datasets were acquired without knowledge of embryo genotype. After imaging was completed, embryos were de-embedded and genotyped. At least 3 timelapse datasets were acquired for all conditions presented.

Image processing and analysis

Image data were processed using ImageJ. Volume rendering was performed using Amira (Visage Imaging) or FluoRender (Wan et al., 2009). Tissue volumes were measured using Amira after manual segmentation based on the membrane channel. Optic stalk cross section area was measured using Amira, after manual (slice by slice) segmentation of the interface between the retina and optic stalk.

Furrow angle measurements—Furrow angle was measured using the ImageJ angle tool. Within the z-stack, the slice containing the greatest optic vesicle area (representing the

dorsal-ventral mid-point of the optic vesicle) was used for the measurement. A 25 μm radius circle was centered at the vertex of the optic stalk furrow. The first point of the angle was selected where the circle intersected with the neural keel, the second point of the angle was the vertex of the optic stalk furrow, and the third point of the angle was selected where the circle intersected with the optic vesicle (shown in Fig. 2F,G).

Invagination angle measurements—Invagination angle was also measured using the ImageJ angle tool. Within the z-stack, the slice containing the greatest lens area (representing the dorsal-ventral mid-point of the lens) was used for the measurement. The first point of the angle was selected at the center of the retina, just behind the lens, the second point of the angle (the vertex) was selected at one outer margin of retina, and the third point of the angle was selected at the other outer margin of the retina (Fig. 2P).

Focal adhesion quantification—Quantification of ECM adhesion using EGFP-vinculin was performed as follows: ratiometric analysis was performed on single confocal slices within the z-stack at the dorsal-ventral midpoint of the optic vesicle (14 hpf, for optic stalk furrow measurements), or at the dorsal-ventral midpoint of the lens (24 hpf, for lens-retina interface measurements). A 25 μm radius circle was centered at the vertex of the optic stalk furrow or deepest point of the lens-retina interface, then fluorescence intensity quantified along the basal surface within that circle (Fig. 3, yellow-bound regions). EGFP-vinculin fluorescence intensity was normalized to mCherry-CAAX intensity within the same area. Enrichment at the optic stalk furrow or lens-retina interface was determined by comparison to similar-sized regions at the brain midline (Fig. 3, blue-bound regions), a place where membrane components might be enriched, though not in an ECM-dependent manner, due to cell constriction at the apical surface.

Basal endfoot width measurements—Basal endfoot width was measured using the same 25 μm radius circles used for measuring EGFP-vinculin enrichment. The number of cells in contact with the basal surfaces within the circles was counted, and basal surfaces lengths were measured using ImageJ. Average basal endfoot width was calculated by dividing the basal surface lengths by the number of cells in contact with the surface.

Box and whisker plots

Box and whisker plots were generated using the ggplot2 package in R. The band inside the box is the median. The upper and lower “hinges” correspond to the first and third quartiles. The upper whisker extends from the upper hinge to the highest value within (1.5 * IQR), where IQR is the inter-quartile range. The lower whisker extends from the lower hinge to the lowest value within (1.5 * IQR). Data points outside of the ends of the whiskers are outliers.

Results

lama1 is required for optic cup formation

In zebrafish, the optic cup forms 12–24 hours post fertilization (hpf), during which time the flat, wing-like optic vesicle transforms into the organized optic cup with morphologically distinct neural retina, retinal pigmented epithelium (RPE), and lens. To determine whether

laminin-α1 is required for optic cup formation, we examined the *bashful*^{UW1} (*bal*^{UW1}) mutant, which harbors a splice donor mutation in the *laminin-α1 (lama1)* gene, resulting in a protein truncation at amino acid 1424 followed by 60 additional amino acids translated from the intron (Paulus and Halloran, 2006; Semina et al., 2006). We refer to this allele as *lama1*^{UW1}. Mutant and sibling control embryos were labeled ubiquitously for membranes (EGFP-CAAX) and chromatin (H2A.F/Z-mCherry) using RNA injection at the 1-cell stage, and 4-dimensional timelapse confocal microscopy was performed from 12.5 to 24 hpf. This time period encompasses optic cup morphogenesis subsequent to optic vesicle evagination. Timelapse datasets reveal a striking disruption of optic cup morphogenesis (Fig. 1A–H; Movies S1, S2). At 12.5 hpf, the mutant optic vesicle appeared rounder and more symmetric along the anterior-posterior axis than the control (Fig. 1A,E). As optic cup morphogenesis proceeded, in control embryos, the neural retina progenitors elongated and took on a stereotypical columnar epithelial morphology, while RPE cells flattened. The lens invaginated from the overlying ectoderm and pinched off, forming its characteristic spherical shape (Fig. 1A–D, Movie S1). In *lama1*^{UW1} mutants, even though the RPE appeared to be present and flattened appropriately, the retina appeared disorganized, and the two tissues failed to enwrap the lens. The lens formed from the overlying ectoderm, though it was misshapen and ovoid (Fig. 1E–H, Movie S2). The failure of the neural retina and RPE to enwrap the lens leaves it exposed – similar to the “protruding lens” phenotype seen by stereomicroscope and reported previously for *lamb1* and *lamg1* mutants (Parsons et al., 2002). All phenotypes described throughout this manuscript appear to be 100% penetrant. Any apparent variability in phenotypes is related to the specific optical sections in the figures. For example, in mutant embryos, the retina still curves slightly around the lens in the dorsal domain; an optical section in the more dorsal domain will look as though invagination is less disrupted than in the central or ventral domains.

To determine when and where laminin protein is present, we performed antibody staining for the laminin protein heterotrimer (Fig. 1I–L). We found that laminin protein was present at all basal surfaces of the optic vesicle and lens throughout the stages of optic cup morphogenesis studied here. Therefore, laminin protein is found at the right time and place to be directly affecting optic cup morphogenesis. To determine how the *lama1*^{UW1} mutant allele affects laminin protein accumulation, antibody staining was performed on 12 hpf *lama1*^{UW1} mutants, when the optic vesicle has evaginated. We found that there was no detectable accumulation of laminin protein heterotrimer at the basal surface of the optic vesicle (Fig. 1M). Therefore, combined with the similar phenotype observed in the loss-of-function *lamb1* and *lamg1* mutants (Parsons et al., 2002), we consider this phenotype to be a loss-of-function for *lama1*.

Loss of lama1 leads to multiple defects in optic cup morphogenesis

We set out to quantitatively define the optic cup morphogenesis defects in *lama1*^{UW1} mutants. First, *lama1* mutants isolated in previous, large-scale screens were classified as having a small eye (Malicki et al., 1996). We sought to determine whether the defects in optic cup morphogenesis could be due to changes in eye size. To analyze eye size and shape, 3D volumes of the eye (neural retina + RPE and lens) were visualized and measured after manual segmentation of confocal z-stacks acquired of live embryos. Live imaging was used

to avoid artifactual changes in volume due to fixation. The manually segmented volumes (Fig. 2A–D) revealed gross changes to the shape of the optic cup in *lama1*^{UW1} mutants: the domain of neural retina and RPE was flatter, the lens was ovoid rather than spherical, and the choroid fissure failed to form correctly (Fig. 2B,D; arrow marks choroid fissure in control embryo; asterisk marks missing choroid fissure in mutant). Volumes were measured to determine if there was a significant change in size: we found, somewhat surprisingly, that *lama1*^{UW1} mutants and control siblings had no significant difference in optic cup volume (Fig. 2E), suggesting that at this stage, defects in optic cup morphogenesis are not the result of gross gain or loss of tissue, and that the “small eye” phenotype observed in previous screens might arise later in development, possibly as a result of alterations in retinal neurogenesis.

Next, based on timelapse data, it appeared as though the optic stalk, the connection between the optic cup and the brain, failed to constrict in *lama1*^{UW1} mutants. Optic stalk constriction initiates through formation of a furrow at the posterior portion of the optic vesicle, resulting in a fold in the tissue, which then moves anteriorly. We measured the furrow angle in *lama1*^{UW1} control and mutant embryos, and found that the furrow was significantly more open in mutants than in control embryos (Fig. 2F–H, also see Methods). The open furrow suggests a failure of the tissue folding event that initiates optic stalk formation. To determine whether optic stalk constriction was indeed impaired in *lama1*^{UW1} mutants, we measured the cross-sectional area of the optic stalk at 24 hpf (Fig. 2I–M). The optic stalk cross section was reconstructed via manual segmentation of the interface of the optic cup and stalk (see Methods), and the surface area measured. We found that optic stalk constriction was significantly impaired in *lama1*^{UW1} mutants (Fig. 2M).

Finally, the protruding lens phenotype suggested that retinal invagination was impaired. The invagination angle (α) was measured in *lama1*^{UW1} control and mutant embryos as shown (Fig. 2N–P). We found that invagination was significantly impaired by loss of lama1 (Fig. 2Q).

We conclude that although optic cup size is normal, multiple steps of optic cup morphogenesis are impaired in *lama1*^{UW1} mutants, suggesting that under normal conditions, laminin regulates choroid fissure formation, optic stalk constriction, and optic cup invagination.

Loss of lama1 leads to spatiotemporally distinct effects on focal adhesion assembly

Laminin and other extracellular matrix molecules signal to cells through large protein complexes known as focal adhesions. Focal adhesions are assembled locally within the cell in response to matrix binding, in a mechanical tension-dependent manner. Although the extracellular matrix has been demonstrated to be present surrounding the entire optic vesicle (Hendrix and Zwaan, 1975; Hilfer and Randolph, 1993; Kurkinen et al., 1979; McAvoy, 1981; Parmigiani and McAvoy, 1984; Peterson et al., 1995; Svoboda and O’Shea, 1987; Tuckett and Morriss-Kay, 1986; Wakely, 1977; Webster et al., 1983, 1984), we wondered when and where focal adhesion assembly was occurring during optic cup morphogenesis. Determining spatiotemporal patterns of focal adhesion assembly during optic cup formation

could help to reveal the specific morphogenetic events during which ECM adhesion and signaling might play a critical role.

We initially considered two possibilities: one result might be that focal adhesions are assembled uniformly around the optic vesicle throughout optic cup morphogenesis, reflecting the apparent uniform localization of ECM components such as laminin (Fig. 1I–L). Another possibility is that focal adhesions are assembled at particular sites during certain morphogenetic events, suggesting spatiotemporal specificity, and the simple presence of ECM might not be sufficient to trigger focal adhesion assembly. To begin to determine when and where focal adhesion assembly might be occurring during optic cup morphogenesis, we performed antibody staining for the focal adhesion protein vinculin, which is recruited to nascent focal adhesions in a tension-dependent manner (Carisey et al., 2013; Dumbauld et al., 2013; Grashoff et al., 2010; Humphries et al., 2007; Rubashkin et al., 2014). We initially assayed vinculin localization at two timepoints, 14 hpf and 24 hpf, to determine whether we could visualize sites of focal adhesion assembly, and whether these might be altered in *lama1*^{UW1} mutant embryos. At 14 hpf, weak, somewhat inconsistent recruitment of vinculin to the forming optic stalk region could be seen in control embryos, with no obvious difference in *lama1*^{UW1} mutant embryos (Fig. 3A–D, *orange arrowheads*). At 24 hpf, vinculin appeared to be weakly recruited to the lens-retina interface in control embryos (Fig. 3E), and surprisingly, appeared to be more strongly recruited in *lama1*^{UW1} mutant embryos (Fig. 3F–H, *white arrows*). These data suggest that rather than vinculin being recruited uniformly around the forming optic cup (reflecting the apparent uniform distribution of laminin and other ECM proteins), there might be spatiotemporal specificity to focal adhesion recruitment during optic cup morphogenesis.

While the antibody staining data were suggestive, these experiments were not quantitative, and variability in signal could be caused by minor differences in embryo clearing or embedding. Additionally, no other were timepoints were initially examined during optic cup morphogenesis. Therefore, we set out to assay focal adhesions quantitatively in live embryos. To this end, we used a fusion of EGFP to the focal adhesion protein vinculin, the same protein assayed by antibody staining. To facilitate quantification, RNA encoding EGFP-vinculin was coinjected into embryos along with mCherry-CAAX, a uniform membrane marker used for fluorescence normalization. We found that in control embryos, EGFP-vinculin reported focal adhesion assembly in a spatiotemporally specific manner, similar to what we observed via antibody staining. This further supports the idea that apparently uniform laminin protein distribution does not lead to uniform focal adhesion assembly. Notably, EGFP-vinculin was recruited to the optic stalk furrow at the onset of optic stalk constriction, and the lens-retina interface during invagination (Fig. 3I–L, Movies S3, S5). We then examined how adhesion might be disrupted by loss of lama1 (Fig. 3M–P), and found, surprisingly, distinct changes in vinculin recruitment during each morphogenetic event. In *lama1*^{UW1} mutant embryos, at the optic stalk furrow, EGFP-vinculin recruitment was diminished (Fig. 3N, Movie S4), but in contrast, EGFP-vinculin recruitment appeared increased at the lens-retina interface during invagination (Fig. 3P, Movie S6).

We quantified these results using ratiometric image analysis on selected regions of interest (ROIs) (Fig. 3Q,R,U,V), and determined EGFP-vinculin enrichment by normalizing to

mCherry-CAAX signal, then comparing normalized signal in the ROI to a different control region, in which EGFP-vinculin and other membrane associated components might appear enriched due to apical cell constriction, but in a manner independent of ECM (also see Methods). Our measurements confirm that at the optic stalk furrow, focal adhesion recruitment was diminished in *lama1*^{UW1} mutants (Fig. 3S), suggesting that laminin promotes focal adhesion assembly at the onset of optic stalk constriction. In contrast, focal adhesion recruitment was increased at the lens-retina interface in *lama1*^{UW1} mutant optic cups (Fig. 3W), suggesting that under wildtype conditions, laminin acts to negatively regulate focal adhesion assembly during invagination, either directly or indirectly.

We were concerned that these measurements could be skewed by potential differences in cell morphology or number in the quantified region. It has been reported that constriction of the basal surface of retinal progenitor cells ("basal constriction") underlies optic cup invagination (Martinez-Morales et al., 2009), and such constriction might also occur during optic stalk furrow formation. Since vinculin recruitment to the basal surface is being quantified, a morphological difference in the basal surface between control and mutant embryos (for example, differences in cell crowding or density) might artifactually lead to an apparent change in focal adhesion recruitment. Therefore, we counted the number of cells within the region being quantified, and calculated an average basal endfoot width for control and *lama1*^{UW1} mutant embryos (Fig. S1). During optic stalk furrow formation, we found no significant difference between control and *lama1*^{UW1} mutant average basal endfoot width (Fig. 3T), suggesting that the significant loss of EGFP-vinculin recruitment in *lama1*^{UW1} mutant embryos cannot be due to a significant difference in the number of cells in the quantified region or basal surface cell morphology. During optic cup invagination, however, retinal progenitors in the *lama1*^{UW1} mutant have a larger average basal endfoot width, suggesting that basal constriction is impaired (Fig. 3X). This also suggests that the increased EGFP-vinculin signal observed at the lens-retina interface in the *lama1*^{UW1} mutant (Fig. 3W), cannot merely be due to cell constriction concentrating focal adhesion proteins at the basal surface, rather, there is increased EGFP-vinculin recruitment at the basal surface of each individual cell in the absence of lama1. Further evidence for specificity of these effects comes from quantification of the medial portion of the optic cup, a domain in which we failed to see obvious EGFP-vinculin recruitment (Fig. 3U,V; *magenta regions*). Quantification and normalization of EGFP-vinculin fluorescence in this area indicated very low levels of recruitment in control embryos (1.1-fold enrichment compared to 1.55-fold at the lens-retina interface), and there was no statistically significant difference between control and *lama1*^{UW1} mutant embryos (Fig. 3Y).

We conclude from these data that focal adhesions are assembled in a spatiotemporally specific manner in the early eye: laminin appears to surround the optic vesicle uniformly, yet vinculin is recruited only to a subset of sites where laminin is present. Further, loss of lama1 disrupts focal adhesion assembly in a divergent manner during the morphogenetic events we observed to be disrupted during optic cup morphogenesis, specifically optic stalk furrow formation and invagination (Fig. 2). Our data suggest that under normal conditions, laminin promotes vinculin recruitment and focal adhesion assembly during optic stalk constriction, but surprisingly, negatively modulates it during optic cup invagination. It is possible that this

may be due to direct or indirect effects of loss of laminin, or functional differences in other ECM components present at different sites (see Discussion).

Cell death is not responsible for optic cup morphogenesis defects in lama1 mutants

In both *in vitro* and *in vivo* systems, attachment to the basement membrane or extracellular matrix is required for cell survival (Frisch and Francis, 1994; Juliano et al., 2004). We therefore determined whether loss of lama1 resulted in increased cell death in *lama1*^{UW1} mutants. Antibody staining for activated caspase-3, a marker of programmed cell death, was performed on *lama1*^{UW1} control and mutant embryos. We found that control embryos had little or no detectable cell death at 24 hpf (Fig. 4A–A"), with only a couple of cells positive for activated caspase-3 in the eye region, usually near the site of lens separation from the surface ectoderm. In contrast, *lama1*^{UW1} mutants contained large patches of dying, activated caspase-3-positive cells, which were found in more medial regions of the optic cup, arising from both within and outside of the optic cup (Fig. 4B–B"; *dashed blue lines* outline the optic cup). These cells could originate either from the optic vesicle or neural crest. Within the optic vesicle, notably, this is where focal adhesion assembly was diminished, near the medial optic vesicle, at the boundary between the optic vesicle and prospective brain tissue (Fig. 3J,N,S). Conversely, at the basal retina (the lens-retina interface), where focal adhesion assembly was not lost in *lama1*^{UW1} mutants (Fig. 3L,P,W), we did not see increased cell death (Fig. 4B–B"), suggesting that maintenance of adhesion could be protective against cell death. These results suggest that, similar to other epithelial tissues, optic cup cells are sensitive to loss of extracellular matrix adhesion, and respond by undergoing cell death.

The significant amount of cell death in *lama1*^{UW1} mutants led us to ask whether this could be responsible for the morphogenetic defects observed in optic cup formation. To test this, we injected RNA encoding the apoptosis inhibitor Bcl-xL (Sidi et al., 2008) into 1-cell stage embryos, to determine whether suppression of cell death is sufficient to rescue the morphogenetic defects in *lama1*^{UW1} mutants. We found that expression of Bcl-xL suppressed apoptosis (note almost complete lack of activated caspase-3 positive cells in *lama1*^{UW1} mutants). However, gross morphogenetic defects were still apparent (Fig. 4C–C"), and *lama1*^{UW1} mutant optic cups still failed to undergo invagination, with the neural retina and RPE failing to enwrap the misshapen, ovoid lens.

We also attempted to suppress cell death in *lama1*^{UW1} mutant embryos with a commonly used p53 morpholino oligonucleotide. However, this was ineffective, and high levels of cell death remained (data not shown). Although many cell death pathways are p53-dependent, anoikis, caused by loss of matrix attachment, can be independent of p53 signaling (Chiarugi and Giannoni, 2008; Guadamillas et al., 2011). Therefore, we conclude that laminin is normally required for cell survival and loss of lama1 leads to anoikis (either directly or indirectly), but this is not responsible for the gross optic cup morphogenesis defects observed.

lama1 mutants display normal motile cell behaviors, but tissue-level structural defects arise during invagination

Laminin has been demonstrated to influence single cell behavior and cell migration in a variety of systems (Adams and Watt, 1993; Daley and Yamada, 2013). We therefore sought to visualize single cell behaviors underlying optic cup formation, and whether they are affected by loss of lama1. To visualize single cell behaviors, we utilized the photoactivatable fluorophore Kaede (Ando et al., 2002). In its native state, Kaede emits green fluorescence (excitation maximum 508 nm), but when exposed to UV light, the protein undergoes an irreversible photocleavage and subsequently emits red fluorescence (excitation maximum 572 nm). By photoconverting small groups of cells expressing cytoplasmic Kaede, we were able to watch their individual behavior and movement throughout the process of optic cup morphogenesis using 4D timelapse confocal microscopy.

Using the Kaede photoconversion strategy, we found that retinal progenitors in both *lama1*^{UW1} control and mutant embryos appeared polarized and displayed active lamellipodial-like protrusions (Fig. 5A–L; Movies S7, S8). These protrusions were observed to extend and retract from both ends of the cell and persisted for a significant period of optic cup morphogenesis, ceasing only ~20 hpf, at which point the retinal progenitors lengthened and assumed their stereotypical elongated columnar epithelial morphology. In both control and mutant embryos, retinal progenitors appeared to carry out the same elongation behavior: though absolute cell length was longer in controls than mutants (Fig. 5M), length/width ratio was not significantly different at either 14 or 24 hpf (Fig. 5N). Protrusive activity was observed in both control and mutant embryos, but with one notable difference: in control embryos, active lamellipodial-like protrusions never extended beyond the boundary of the optic vesicle. In *lama1*^{UW1} mutant embryos, we sometimes observed protrusions that extended beyond the boundary of the optic vesicle. These protrusions did not exhibit a characteristic lamellipodial-like morphology, but rather appeared more bleb-like (Fig. 5H', *magenta asterisk*). These were reminiscent of protrusions that extended beyond the limit of the optic vesicle in *lamg1* mutants and morphants during evagination (Ivanovitch et al., 2013). These data suggest that despite the change in overall tissue morphology, the ability to produce motile cell behaviors and undergo cell elongation is not dependent upon lama1.

Despite normal cellular behaviors, a separate, structural phenotype was observed. In control embryos, retinal progenitors aligned with their neighbors, such that their apical and basal ends were in register with each other throughout the course of optic cup morphogenesis (Fig. 5A–F'). In this way, the retina maintained its pseudostratified monolayer structure prior to the onset of neurogenesis. In *lama1*^{UW1} mutant embryos, however, retinal progenitors failed to maintain apicobasal register: though cells were in register during the first part of optic cup morphogenesis, they appeared to sort into separate domains during invagination (Fig. 5G–L'). At the end of optic cup formation, marked retinal progenitors failed to span the width of the retina (Fig. 5L'). This may be better visualized when moving through a confocal z-stack of *lama1*^{UW1} control and mutant optic cups at 24 hpf (Movies S9, S10). In control embryos, retinal progenitor cells were oriented with their long axes pointing toward the lens (Fig. 1D, Movie S9). In contrast, in *lama1*^{UW1} mutant embryos, cells appeared to be organized into multiple domains; cells in some domains appeared to be oriented with their long axes not

pointing toward the lens (Fig. 1H, Movie S10). Therefore, lama1 is required to maintain correct retinal structure and orientation of progenitor elongation through optic cup invagination, though it does not appear to be required for retinal progenitors to produce protrusive cell behaviors and elongate.

Apicobasal polarity is disrupted in lama1 mutants

Laminin has been demonstrated to be critical for establishing and maintaining epithelial polarity both *in vitro* and *in vivo* (Martin-Belmonte and Mostov, 2008). At early stages of zebrafish optic vesicle evagination, ZO-1, a component of tight junctions, is localized to the apical surface, opposite the laminin staining that surrounds the optic vesicle (Ivanovitch et al., 2013). It was shown that during optic vesicle evagination, laminin is important for establishing apicobasal polarity: in the *lamg1* mutant (*sleepy*^{m86}), ZO-1 was mislocalized to what should be the presumptive basal surface, in addition to the apparent apical surface (Ivanovitch et al., 2013). In that study, however, polarity was assayed specifically during optic vesicle evagination stages; it is unknown how epithelial polarity and structure might change throughout the process of optic cup morphogenesis in the presence or absence of laminin.

Therefore, we first assayed polarity at the completion of optic cup morphogenesis (24 hpf), in both *lama1*^{UW1} control and mutant embryos. To do this, antibody staining was performed for a marker of the apical surface, atypical protein kinase C (aPKC). We found that in control embryos, aPKC was localized to a single apical surface, at the interface between the neural retina and retinal pigmented epithelium (Fig. 6A, *green arrowhead*). In *lama1*^{UW1} mutant embryos, however, localization of aPKC was disrupted. Though polarity was disrupted with 100% penetrance, the exact number of apical domains present was variable (Fig. 6B–D): in addition to the correct apical domain (*green arrowheads*), multiple ectopic domains of aPKC localization were found (*yellow arrowheads*), as well as ectopic puncta (*magenta asterisks*). The ectopic domains and puncta were scattered throughout the retina. Similar results were obtained using an antibody against the tight junction protein ZO-1 (data not shown). These observations suggest that early defects in cell polarity that are caused by loss of laminin proteins may persist through optic cup morphogenesis, resulting in multiple, randomly positioned apical domains in the optic cup.

To determine how these multiple domains might arise and change over time, we took a 4-dimensional live imaging approach (Fig. 6E–P, Movies S11, S12), visualizing the apical surface using pard3-GFP, a fusion of the zebrafish homolog of the polarity protein pard3 to GFP (Geldmacher-Voss et al., 2003). Embryos were injected at the one-cell stage with RNA encoding pard3-GFP.

At 13 hpf, in control embryos, pard3-GFP marked a coherent, single apical surface lining the lumen of the optic vesicle (the interface between the two layers of the optic vesicle) (Fig. 6E). As optic cup morphogenesis proceeded, the single apical domain remained intact, extending along the forming retina-RPE interface as the optic vesicle elongated and subsequently underwent invagination (Fig. 6E–J, Movie S11). At 24 hpf, the apical localization of pard3-GFP is very similar to that of aPKC (Fig. 6A,J). Thus, the apical

domain that initially demarcates the layers of the optic vesicle comes to form the interface between the retinal pigmented epithelium and neural retina in the optic cup.

In the *lama1*^{UW1} mutant, we found that apicobasal polarity was severely disrupted throughout optic cup morphogenesis. At 13 hpf, the optic vesicle was already slightly misshapen (similar to Fig. 1E). Apical identity was disrupted: pard3-GFP was found with a diffuse cytoplasmic localization and also in puncta scattered randomly throughout cells of the optic vesicle (Fig. 6K). As optic cup morphogenesis proceeded, the diffuse cytoplasmic pard3-GFP fluorescence gradually disappeared (by 22.2 hpf, Fig. 6O). Coherent domains of pard3-GFP fluorescence appeared to form and coalesce stochastically (Fig. 6K–P, Movie S12). By the end of optic cup morphogenesis, pard3-GFP localization resolved into multiple apical domains, similar to what we observed by aPKC antibody staining (Fig. 6B–D,P). In the particular embryo shown in Fig. 6P, pard3-GFP was observed at both the correct location (the interface between the neural retina and retinal pigmented epithelium, *green arrowhead*), as well as at ectopic locations: at the interface between the neural retina and lens, and also in a domain extending into the middle of the retina (*yellow arrowheads*). We conclude that laminin is required for epithelial polarity: in the absence of lama1, cell polarity is disrupted throughout the process of optic cup morphogenesis, with cells randomly designating apical identity and self-organizing stochastically to generate multiple apical domains.

Discussion

It has been long known that a rich extracellular matrix layer surrounds the eye throughout the process of optic cup morphogenesis (Hendrix and Zwaan, 1975; Hilfer and Randolph, 1993; Kurkinen et al., 1979; McAvoy, 1981; Parmigiani and McAvoy, 1984; Peterson et al., 1995; Svoboda and O'Shea, 1987; Tuckett and Morriss-Kay, 1986; Wakely, 1977; Webster et al., 1983, 1984), yet in most cases, the function of specific matrix components in regulating the morphogenetic process remains unclear. Here, we demonstrate that laminin extracellular matrix regulates spatiotemporally specific focal adhesion assembly, cell survival, cellular protrusions, and cell polarity during optic cup morphogenesis. Programmed cell death, likely anoikis due to the loss of substrate attachment, is clearly induced, yet it appears to be separate from the morphogenetic phenotypes, as inhibition of cell death does not rescue optic cup formation. Previous work focusing on optic vesicle evagination demonstrated that laminin is critical for tissue organization, establishing cell polarity, and delimiting protrusive activity (Ivanovitch et al., 2013). Here, we have extended those observations to determine the role of laminin through the process of optic cup formation, using a combination of genetics and 4-dimensional live imaging. Future work will aim to determine the specific molecular mechanisms by which laminin controls these diverse cellular processes.

Although the complex extracellular matrix layer has been described to surround the developing eye in every vertebrate organism tested to date, how this affects focal adhesion assembly – the output of functional extracellular matrix engagement – has been unclear. Using vinculin antibody staining and 4D live imaging of EGFP-vinculin, we find that rather than reflecting the apparent uniform distribution of laminin around the optic vesicle, focal adhesions are assembled in a spatiotemporally specific manner, primarily during optic stalk

constriction and optic cup invagination. Further, removal of lama1 results in surprisingly divergent effects: focal adhesion assembly is decreased during optic stalk furrow formation, but increased during optic vesicle invagination. We propose that the changes in adhesion disrupt both morphogenetic processes. While we would have predicted that focal adhesions might be decreased by loss of laminin, the increase during invagination is more surprising. We hypothesize that differential interactions between ECM components and receptors may underlie the apparently variable role of laminin in modulating adhesion.

Our experiments do not indicate whether these effects due to loss of laminin are direct or indirect. Laminin is not, of course, the only extracellular matrix component present lining the basal surface of the developing eye. In all vertebrates examined to date, laminin, fibronectin, and collagen surround the developing optic vesicle and lens, in addition to the host of other glycoproteins also found in the complex matrix. Their specific functions in optic cup morphogenesis are unclear, though loss of one component may impact the expression and function of other components. Our initial experiments indicate that loss of lama1 results in disruption of the uniform fibronectin matrix around the anterior lens of the optic cup at 24 hpf, though no gross changes around the rest of the optic vesicle or cup are apparent at either 14 hpf or 24 hpf (data not shown). Thus, although loss of fibronectin in the *lama1*^{UW1} mutant does occur in a spatiotemporally specific manner, obvious changes in fibronectin localization are not found in regions where vinculin recruitment is affected, specifically at the optic stalk furrow or lens-retina interface. There is a possibility that loss of laminin leads to more subtle changes in ECM structure, for example, fibronectin fibril assembly; future experiments will address these possibilities. It is known that vinculin is recruited to focal adhesions in a manner that is facilitated by tissue tension and ECM stiffness (Pasapera et al., 2010). We speculate that during optic cup invagination, laminin may serve to limit the stiffness and higher order assembly of collagen and fibronectin networks, thereby limiting vinculin recruitment and focal adhesion assembly under normal conditions.

One other structural defect we observed is that of the oblong lens (Fig. 1). Instead of invaginating and forming a spherical structure, the lens has a flattened, ovoid shape. The lens volume is unchanged (Fig. 2E), so specification and proliferation are unlikely to be affected. We hypothesize that an intact laminin extracellular matrix is required to establish uniform circumferential tension around the invaginating lens: loss of adhesion to the laminin matrix between the prospective lens and retina results in a loss of tension in the anterior-posterior axis, resulting in the oblong lens. In addition, it is known that laminin is required for later steps of lens development: lama1 mutants display lens degeneration or extrusion (Pathania et al., 2014; Semina et al., 2006). It is possible that these early defects in establishment of the proper lens structure directly impact these later phenotypes. It has been previously reported that at later stages, focal adhesions are decreased in the anterior segment of *lama1* mutant embryos (Semina et al., 2006); this decrease could be initiated early due to loss of both laminin and fibronectin (data not shown).

We propose the following model for laminin activity during optic cup formation (Fig. 7). In wild type embryos, laminin surrounds the optic vesicle throughout morphogenesis stages. Epithelial polarity is established by the end of evagination, and the single, coherent apical

domain (separating the two layers of the optic vesicle) is reshaped as the optic vesicle undergoes elongation and invagination to form the optic cup. Focal adhesions are assembled during optic stalk furrow formation and at the lens-retina interface during invagination. Laminin promotes focal adhesion assembly during optic stalk constriction, but may negatively modulate it during optic cup invagination.

The analyses performed here, as well as detailed cellular analyses performed by other groups, have begun to inform a detailed functional role for laminin in optic cup morphogenesis. In the future, it will be important to both dissect the specific functions of each extracellular matrix component and determine how each affects the function of others in this complex morphogenetic process.

Supplementary Material

Refer to Web version on PubMed Central for supplementary material.

Acknowledgments

We are grateful to Mary Halloran, Brian Link, Alexander Reugels, Adam Navis, and Michel Bagnat for reagents. Thanks to Jennifer Gutzman and members of the Chien and Kwan Labs for useful discussions, and Mark Metzstein and Charlie Murtaugh for critical reading of the manuscript. This work was initially supported by a postdoctoral fellowship to K.M.K. from the American Cancer Society, and subsequently by grants to K.M.K. from the Knights Templar Eye Foundation, a March of Dimes Basil O'Connor Starter Scholar Award, and NEI/NIH (R01 EY025378, R01 EY025780). C.D.B. was supported by the University of Utah Developmental Biology Training Grant (NIH T32HD007491).

References

Adams JC, Watt FM. Regulation of development and differentiation by the extracellular matrix. Development. 1993; 117:1183–1198. [PubMed: 8404525]

Ando R, Hama H, Yamamoto-Hino M, Mizuno H, Miyawaki A. An optical marker based on the UV-induced green-to-red photoconversion of a fluorescent protein. Proc Natl Acad Sci U S A. 2002; 99:12651–12656. [PubMed: 12271129]

Biehlmaier O, Makhankov Y, Neuhauss SC. Impaired retinal differentiation and maintenance in zebrafish laminin mutants. Invest Ophthalmol Vis Sci. 2007; 48:2887–2894. [PubMed: 17525225]

Carisey A, Tsang R, Greiner AM, Nijenhuis N, Heath N, Nazgiewicz A, Kemkemer R, Derby B, Spatz J, Ballestrem C. Vinculin regulates the recruitment and release of core focal adhesion proteins in a force-dependent manner. Curr Biol. 2013; 23:271–281. [PubMed: 23375895]

Chiarugi P, Giannoni E. Anoikis: a necessary death program for anchorage-dependent cells. Biochem Pharmacol. 2008; 76:1352–1364. [PubMed: 18708031]

Chow RL, Lang RA. Early eye development in vertebrates. Annu Rev Cell Dev Biol. 2001; 17:255–296. [PubMed: 11687490]

Colognato H, Yurchenco PD. Form and function: the laminin family of heterotrimers. Dev Dyn. 2000; 218:213–234. [PubMed: 10842354]

Daley WP, Yamada KM. ECM-modulated cellular dynamics as a driving force for tissue morphogenesis. Curr Opin Genet Dev. 2013; 23:408–414. [PubMed: 23849799]

Dumbauld DW, Lee TT, Singh A, Scrimgeour J, Gersbach CA, Zamir EA, Fu J, Chen CS, Curtis JE, Craig SW, Garcia AJ. How vinculin regulates force transmission. Proc Natl Acad Sci U S A. 2013; 110:9788–9793. [PubMed: 23716647]

England SJ, Blanchard GB, Mahadevan L, Adams RJ. A dynamic fate map of the forebrain shows how vertebrate eyes form and explains two causes of cyclopia. Development. 2006; 133:4613–4617. [PubMed: 17079266]

Frisch SM, Francis H. Disruption of epithelial cell-matrix interactions induces apoptosis. J Cell Biol. 1994; 124:619–626. [PubMed: 8106557]

Fuhrmann S. Eye morphogenesis and patterning of the optic vesicle. Curr Top Dev Biol. 2010; 93:61–84. [PubMed: 20959163]

Geldmacher-Voss B, Reugels AM, Pauls S, Campos-Ortega JA. A 90-degree rotation of the mitotic spindle changes the orientation of mitoses of zebrafish neuroepithelial cells. Development. 2003; 130:3767–3780. [PubMed: 12835393]

Grant PK, Moens CB. The neuroepithelial basement membrane serves as a boundary and a substrate for neuron migration in the zebrafish hindbrain. Neural Dev. 2010; 5:9. [PubMed: 20350296]

Grashoff C, Hoffman BD, Brenner MD, Zhou R, Parsons M, Yang MT, McLean MA, Sligar SG, Chen CS, Ha T, Schwartz MA. Measuring mechanical tension across vinculin reveals regulation of focal adhesion dynamics. Nature. 2010; 466:263–266. [PubMed: 20613844]

Guadamillas MC, Cerezo A, Del Pozo MA. Overcoming anoikis--pathways to anchorage-independent growth in cancer. J Cell Sci. 2011; 124:3189–3197. [PubMed: 21940791]

Heermann S, Schutz L, Lemke S, Krieglstein K, Wittbrodt J. Eye morphogenesis driven by epithelial flow into the optic cup facilitated by modulation of bone morphogenetic protein. Elife. 2015:4.

Hendrix RW, Zwaan J. The matrix of the optic vesicle-presumptive lens interface during induction of the lens in the chicken embryo. J Embryol Exp Morphol. 1975; 33:1023–1049. [PubMed: 1176872]

Hilfer SR, Randolph GJ. Immunolocalization of basal lamina components during development of chick otic and optic primordia. Anat Rec. 1993; 235:443–452. [PubMed: 8430914]

Humphries JD, Wang P, Streuli C, Geiger B, Humphries MJ, Ballestrem C. Vinculin controls focal adhesion formation by direct interactions with talin and actin. J Cell Biol. 2007; 179:1043–1057. [PubMed: 18056416]

Ivanovitch K, Cavodeassi F, Wilson SW. Precocious acquisition of neuroepithelial character in the eye field underlies the onset of eye morphogenesis. Dev Cell. 2013; 27:293–305. [PubMed: 24209576]

Jiang YJ, Brand M, Heisenberg CP, Beuchle D, Furutani-Seiki M, Kelsh RN, Warga RM, Granato M, Haffter P, Hammerschmidt M, Kane DA, Mullins MC, Odenthal J, van Eeden FJ, Nusslein-Volhard C. Mutations affecting neurogenesis and brain morphology in the zebrafish, Danio rerio. Development. 1996; 123:205–216. [PubMed: 9007241]

Juliano RL, Reddig P, Alahari S, Edin M, Howe A, Aplin A. Integrin regulation of cell signalling and motility. Biochem Soc Trans. 2004; 32:443–446. [PubMed: 15157156]

Karlstrom RO, Trowe T, Klostermann S, Baier H, Brand M, Crawford AD, Grunewald B, Haffter P, Hoffmann H, Meyer SU, Muller BK, Richter S, van Eeden FJ, Nusslein-Volhard C, Bonhoeffer F. Zebrafish mutations affecting retinotectal axon pathfinding. Development. 1996; 123:427–438. [PubMed: 9007260]

Kimmel CB, Ballard WW, Kimmel SR, Ullmann B, Schilling TF. Stages of embryonic development of the zebrafish. Dev Dyn. 1995; 203:253–310. [PubMed: 8589427]

Kurkinen M, Alitalo K, Vaheri A, Stenman S, Saxen L. Fibronectin in the development of embryonic chick eye. Dev Biol. 1979; 69:589–600. [PubMed: 437354]

Kwan KM, Otsuna H, Kidokoro H, Carney KR, Saijoh Y, Chien CB. A complex choreography of cell movements shapes the vertebrate eye. Development. 2012; 139:359–372. [PubMed: 22186726]

Lee J, Gross JM. Laminin beta1 and gamma1 containing laminins are essential for basement membrane integrity in the zebrafish eye. Invest Ophthalmol Vis Sci. 2007; 48:2483–2490. [PubMed: 17525174]

Malicki J, Neuhauss SC, Schier AF, Solnica-Krezel L, Stemple DL, Stainier DY, Abdelilah S, Zwartkruis F, Rangini Z, Driever W. Mutations affecting development of the zebrafish retina. Development. 1996; 123:263–273. [PubMed: 9007246]

Martin-Belmonte F, Mostov K. Regulation of cell polarity during epithelial morphogenesis. Curr Opin Cell Biol. 2008; 20:227–234. [PubMed: 18282696]

Martinez-Morales JR, Rembold M, Greger K, Simpson JC, Brown KE, Quiring R, Pepperkok R, Martin-Bermudo MD, Himmelbauer H, Wittbrodt J. ojoplano-mediated basal constriction is essential for optic cup morphogenesis. Development. 2009; 136:2165–2175. [PubMed: 19502481]

Martinez-Morales JR, Wittbrodt J. Shaping the vertebrate eye. Curr Opin Genet Dev. 2009; 19:511–517. [PubMed: 19819125]

McAvoy JW. The spatial relationship between presumptive lens and optic vesicle/cup during early eye morphogenesis in the rat. Exp Eye Res. 1981; 33:447–458. [PubMed: 7197633]

Miner JH, Yurchenco PD. Laminin functions in tissue morphogenesis. Annu Rev Cell Dev Biol. 2004; 20:255–284. [PubMed: 15473841]

Parmigiani C, McAvoy J. Localisation of laminin and fibronectin during rat lens morphogenesis. Differentiation. 1984; 28:53–61. [PubMed: 6394411]

Parsons MJ, Pollard SM, Saude L, Feldman B, Coutinho P, Hirst EM, Stemple DL. Zebrafish mutants identify an essential role for laminins in notochord formation. Development. 2002; 129:3137–3146. [PubMed: 12070089]

Pasapera AM, Schneider IC, Rericha E, Schlaepfer DD, Waterman CM. Myosin II activity regulates vinculin recruitment to focal adhesions through FAK-mediated paxillin phosphorylation. J Cell Biol. 2010; 188:877–890. [PubMed: 20308429]

Pathania M, Semina EV, Duncan MK. Lens extrusion from Laminin alpha 1 mutant zebrafish. ScientificWorldJournal. 2014; 2014:524929. [PubMed: 24526906]

Paulus JD, Halloran MC. Zebrafish bashful/laminin-alpha 1 mutants exhibit multiple axon guidance defects. Dev Dyn. 2006; 235:213–224. [PubMed: 16261616]

Peterson PE, Pow CS, Wilson DB, Hendrickx AG. Localisation of glycoproteins and glycosaminoglycans during early eye development in the macaque. J Anat. 1995; 186(Pt 1):31–42. [PubMed: 7649817]

Picker A, Cavodeassi F, Machate A, Bernauer S, Hans S, Abe G, Kawakami K, Wilson SW, Brand M. Dynamic coupling of pattern formation and morphogenesis in the developing vertebrate retina. PLoS Biol. 2009; 7:e1000214. [PubMed: 19823566]

Pollard SM, Parsons MJ, Kamei M, Kettleborough RN, Thomas KA, Pham VN, Bae MK, Scott A, Weinstein BM, Stemple DL. Essential and overlapping roles for laminin alpha chains in notochord and blood vessel formation. Dev Biol. 2006; 289:64–76. [PubMed: 16321372]

Rembold M, Loosli F, Adams RJ, Wittbrodt J. Individual cell migration serves as the driving force for optic vesicle evagination. Science. 2006; 313:1130–1134. [PubMed: 16931763]

Rubashkin MG, Cassereau L, Bainer R, DuFort CC, Yui Y, Ou G, Paszek MJ, Davidson MW, Chen YY, Weaver VM. Force engages vinculin and promotes tumor progression by enhancing PI3K activation of phosphatidylinositol (3,4,5)-triphosphate. Cancer Res. 2014; 74:4597–4611. [PubMed: 25183785]

Schier AF, Neuhauss SC, Harvey M, Malicki J, Solnica-Krezel L, Stainier DY, Zwartkruis F, Abdelilah S, Stemple DL, Rangini Z, Yang H, Driever W. Mutations affecting the development of the embryonic zebrafish brain. Development. 1996; 123:165–178. [PubMed: 9007238]

Semina EV, Bosenko DV, Zinkevich NC, Soules KA, Hyde DR, Vihtelic TS, Willer GB, Gregg RG, Link BA. Mutations in laminin alpha 1 result in complex, lens-independent ocular phenotypes in zebrafish. Dev Biol. 2006; 299:63–77. [PubMed: 16973147]

Sidi S, Sanda T, Kennedy RD, Hagen AT, Jette CA, Hoffmans R, Pascual J, Imamura S, Kishi S, Amatruda JF, Kanki JP, Green DR, DAndrea AA, Look AT. Chk1 suppresses a caspase-2 apoptotic response to DNA damage that bypasses p53, Bcl-2, and caspase-3. Cell. 2008; 133:864–877. [PubMed: 18510930]

Sittaramane V, Sawant A, Wolman MA, Maves L, Halloran MC, Chandrasekhar A. The cell adhesion molecule Tag1, transmembrane protein Stbm/Vangl2, and Lamininalpha1 exhibit genetic interactions during migration of facial branchiomotor neurons in zebrafish. Dev Biol. 2009; 325:363–373. [PubMed: 19013446]

Svoboda KK, O'Shea KS. An analysis of cell shape and the neuroepithelial basal lamina during optic vesicle formation in the mouse embryo. Development. 1987; 100:185–200. [PubMed: 3652969]

Sztal TE, Sonntag C, Hall TE, Currie PD. Epistatic dissection of laminin-receptor interactions in dystrophic zebrafish muscle. Hum Mol Genet. 2012; 21:4718–4731. [PubMed: 22859503]

Tuckett F, Morriss-Kay GM. The distribution of fibronectin, laminin and entactin in the neurulating rat embryo studied by indirect immunofluorescence. J Embryol Exp Morphol. 1986; 94:95–112. [PubMed: 3531379]

Wakely J. Scanning electron microscope study of the extracellular matrix between presumptive lens and presumptive retina of the chick embryo. Anat Embryol (Berl). 1977; 150:163–170. [PubMed: 855939]

Wan Y, Otsuna H, Chien CB, Hansen C. An interactive visualization tool for multi-channel confocal microscopy data in neurobiology research. IEEE Trans Vis Comput Graph. 2009; 15:1489–1496. [PubMed: 19834225]

Webster EH Jr, Silver AF, Gonsalves NI. Histochemical analysis of extracellular matrix material in embryonic mouse lens morphogenesis. Dev Biol. 1983; 100:147–157. [PubMed: 6194023]

Webster EH Jr, Silver AF, Gonsalves NI. The extracellular matrix between the optic vesicle and presumptive lens during lens morphogenesis in an anophthalmic strain of mice. Dev Biol. 1984; 103:142–150. [PubMed: 6201404]

Wolman MA, Sittaramane VK, Essner JJ, Yost HJ, Chandrasekhar A, Halloran MC. Transient axonal glycoprotein-1 (TAG-1) and laminin-alpha1 regulate dynamic growth cone behaviors and initial axon direction in vivo. Neural Dev. 2008; 3:6. [PubMed: 18289389]

Yang XJ. Roles of cell-extrinsic growth factors in vertebrate eye pattern formation and retinogenesis. Semin Cell Dev Biol. 2004; 15:91–103. [PubMed: 15036212]

Zinkevich NS, Bosenko DV, Link BA, Semina EV. laminin alpha 1 gene is essential for normal lens development in zebrafish. BMC Dev Biol. 2006; 6:13. [PubMed: 16522196]

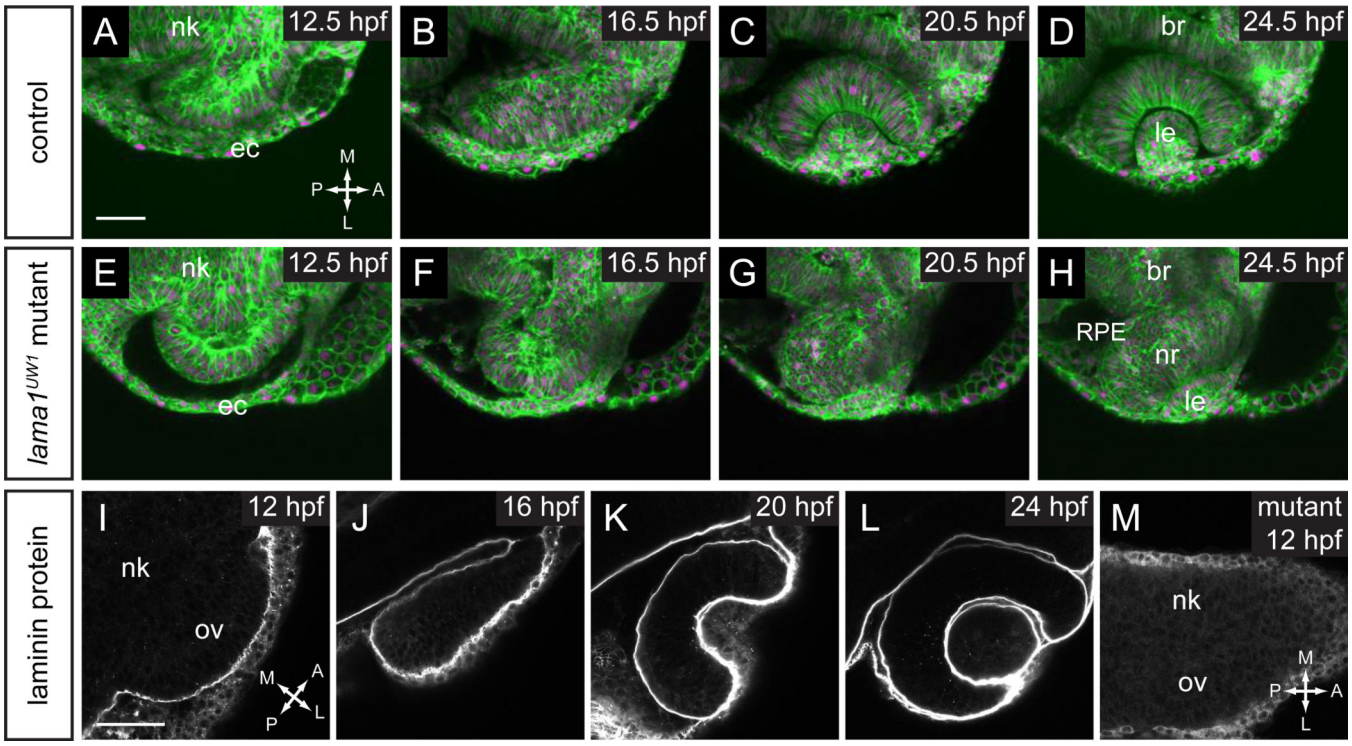

Figure 1.

Timelapse confocal microscopy reveals severe defects in optic cup formation in *lama1*^{UW1} mutant.

(A–H) Single confocal slices from 4D datasets of optic vesicle morphogenesis, 12.5–24.5 hpf. EGFP-CAAX (membranes, *green*), H2A.F/Z-mCherry (nuclei, *magenta*).

(A–D) Optic cup formation in control embryo. (E–H) Optic cup formation in *lama1*^{UW1} mutant embryo. Dorsal views; scale bar, 50 μm.

(I–M) Localization of laminin protein. (I–L) In control embryos, laminin protein is found lining basal surfaces of developing eye and brain. (M) *lama1*^{UW1} mutant embryo reveals absence of laminin protein from early stages of optic vesicle development.

nk, neural keel; *ov*, optic vesicle; *ec*, ectoderm; *br*, brain; *RPE*, retinal pigmented epithelium; *nr*, neural retina; *le*, lens. A, anterior; P, posterior; M, medial; L, lateral.

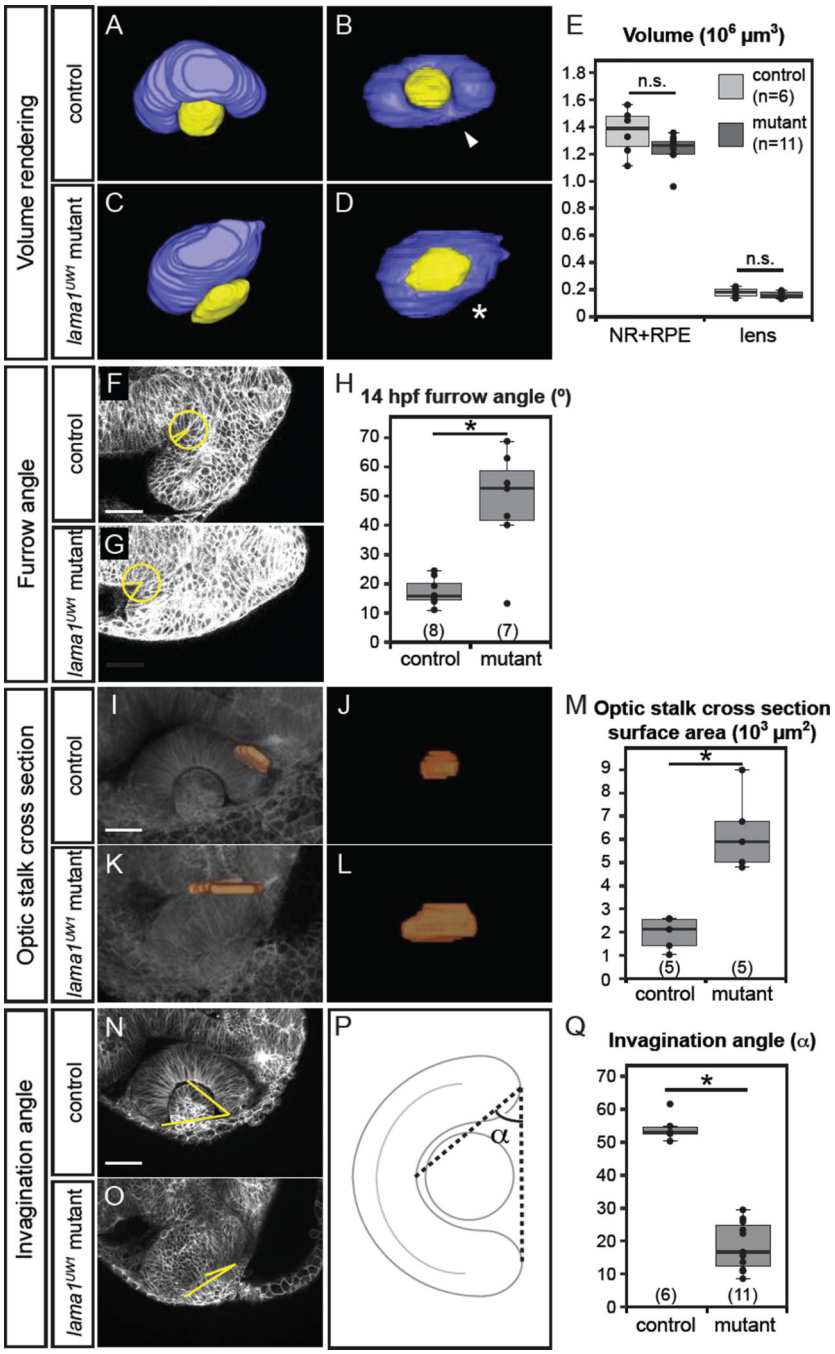

Figure 2.

Quantitative analysis of *lama1*^{UW1} mutant phenotype.

(A–E) Analysis of eye size at 24 hpf. (A–D) Volume renderings of control (A,B) and mutant (C,D) eyes. Neural retina + RPE (*blue*), lens (*yellow*). (A,C) Dorsal views. (B,D) Lateral views. *arrowhead*, choroid fissure; *asterisk*, choroid fissure missing in mutant. (E) Quantification of optic cup and lens volume in control and mutant eyes shows no significant difference in eye size.

(F–H) Quantification of furrow angle during initial stages of optic stalk constriction. Single confocal section of control (F) and mutant (G) embryos, membrane channel (*gray*) at 14 hpf. A circle with a 25 μm radius was placed with its center at the vertex of the furrow, and angle was calculated by drawing radii to positions at which the circle intersected the optic vesicle and brain neuroepithelium. (H) Quantification of furrow angle demonstrates that the furrow exhibits a significantly larger angle in *lama1*^{UW1} mutants.

(I–M) Visualization and quantification of optic stalk constriction. (I–L) 3D rendering of optic stalk cross-section (*orange*) over membrane channel (*gray*) at 24 hpf. (I,K) Dorsal views. (J,L) Face-on views of the optic stalk cross section. (M) Quantification of optic stalk cross section area shows that optic stalk constriction is impaired in *lama1*^{UW1} mutant embryos.

(N–Q) Quantification of invagination angle. (N,O) Single confocal images of membrane channel (gray) in *lama1*^{UW1} control (N) and mutant (O) eyes at 24 hpf. Lines (*yellow*) were drawn to determine angle of invagination. (P) Schematic demonstrating how invagination angle (α) was determined. (Q) Quantification of invagination angle shows a severe defect in invagination in *lama1*^{UW1} mutant embryos.

numbers at base of graph show embryos scored (one eye each); *P<0.001, using the student's t-test.

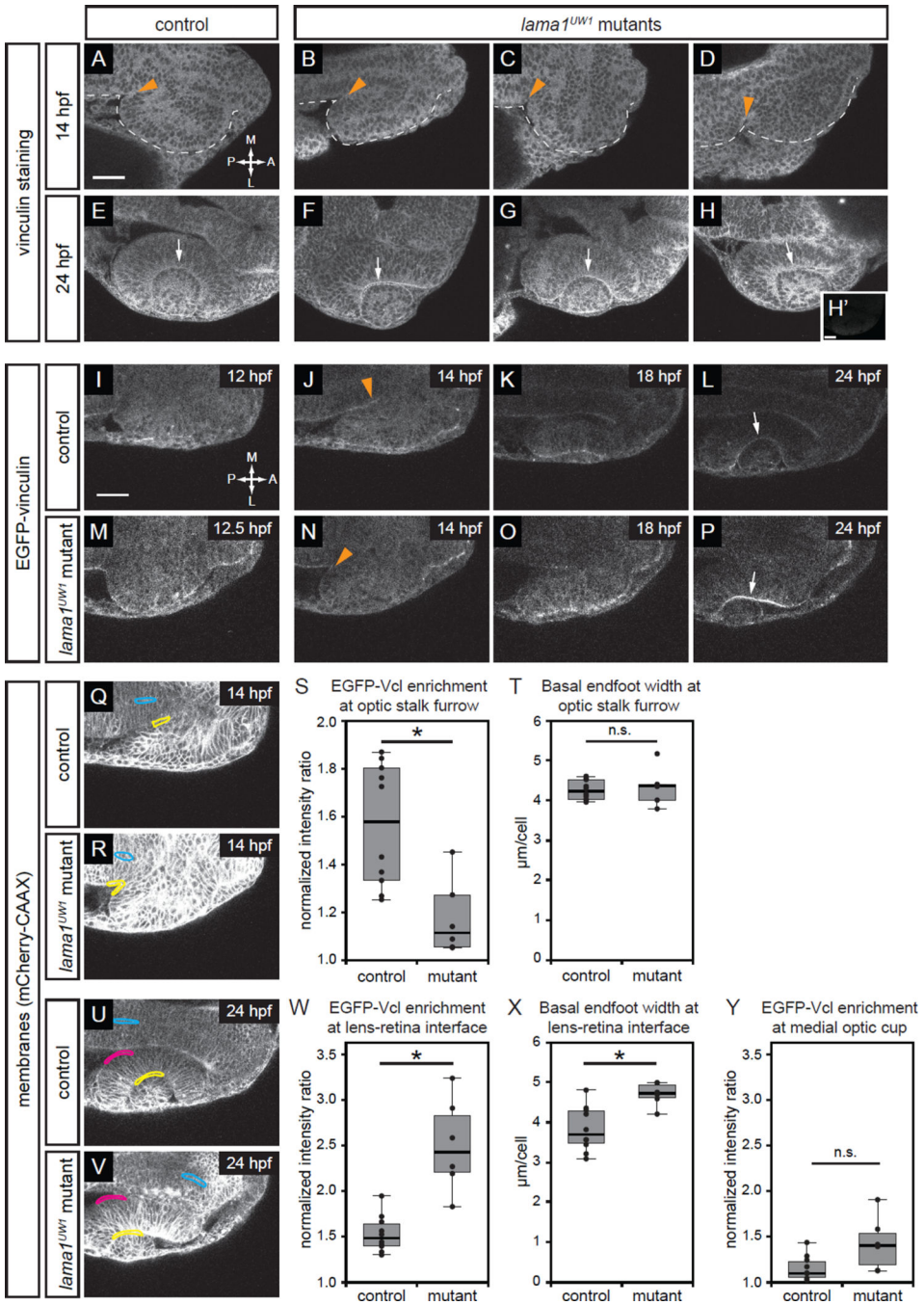

Figure 3.

Focal adhesions are assembled in a specific spatiotemporal pattern, and are differentially disrupted by loss of lama1.

(A–H) Antibody staining for the focal adhesion protein vinculin at 14 hpf (A–D) or 24 hpf (E–H), in control (A,E) or *lama1*^{UW1} mutant (B-D, F-H) embryos. (H') No primary anti-vinculin antibody control. *Orange arrowheads*, location of optic stalk furrow; *white arrows*, lens-retina interface; *dashed line*, outline of optic vesicle.

(I–P) Single confocal slices from 4D datasets of EGFP-vinculin (*grayscale*) localization during optic cup morphogenesis, ~12–24 hpf.

(I–L) EGFP-vinculin recruitment in control embryo is apparent at the optic stalk furrow (J, *orange arrowhead*), and lens-retina interface (L, *white arrow*). (M–P) EGFP-vinculin recruitment in *lama1*^{UW1} mutant embryo at the optic stalk furrow (N, *orange arrowhead*), and lens-retina interface (P, *white arrow*).

Dorsal views; scale bar, 50 μm. A, anterior; P, posterior; M, medial; L, lateral. (Q–Y) Quantification of EGFP-vinculin recruitment at the optic stalk furrow and lens-retina interface. (Q,R,U,V) mCherry-CAAX (membranes, *gray*) localization in same single confocal slices as J,N,L,P, respectively. At the optic stalk furrow or lens-retina interface (Q,R,U,V; *yellow regions*), EGFP-vinculin fluorescence intensity was normalized to mCherry-CAAX. Enrichment was measured by comparing to normalized EGFP-vinculin fluorescence intensity at the midline (Q,R,U,V; *cyan regions*). A control medial optic cup domain (U,V; *magenta regions*) was quantified as a location where EGFP-vinculin recruitment was not noted; this domain was also compared to normalized EGFP-vinculin fluorescence intensity at the midline (U,V; *cyan regions*). (S) Quantification of EGFP-vinculin recruitment indicates decreased ECM adhesion at the optic stalk furrow in the *lama1*^{UW1} mutant. (T) Average basal endfoot width at the optic stalk furrow, based on counting the number of cells within the quantified region; no significant difference indicates that differences in cell morphology at that position (e.g. basal constriction) cannot strictly account for differences in apparent EGFP-vinculin recruitment. (W) Quantification of EGFP-vinculin recruitment indicates increased ECM adhesion at the lens-retina interface in the *lama1*^{UW1} mutant. (X) Average basal endfoot width at the lens-retina interface, based on counting the number of cells within the quantified region; *lama1*^{UW1} mutants have fewer cells with wider basal surfaces, indicating that increased cell number or constriction cannot account for apparent increased EGFP-vinculin recruitment at the mutant basal surface. (Y) Quantification of EGFP-vinculin recruitment at a control site in the medial optic cup where no enrichment of vinculin recruitment occurred in control or *lama1*^{UW1} mutants. Quantifications were performed on 10 control embryos and 6 mutant embryos (one eye scored per embryo); n.s., not significant; $*P<0.005$, using a two-tailed t-test of unequal variance.

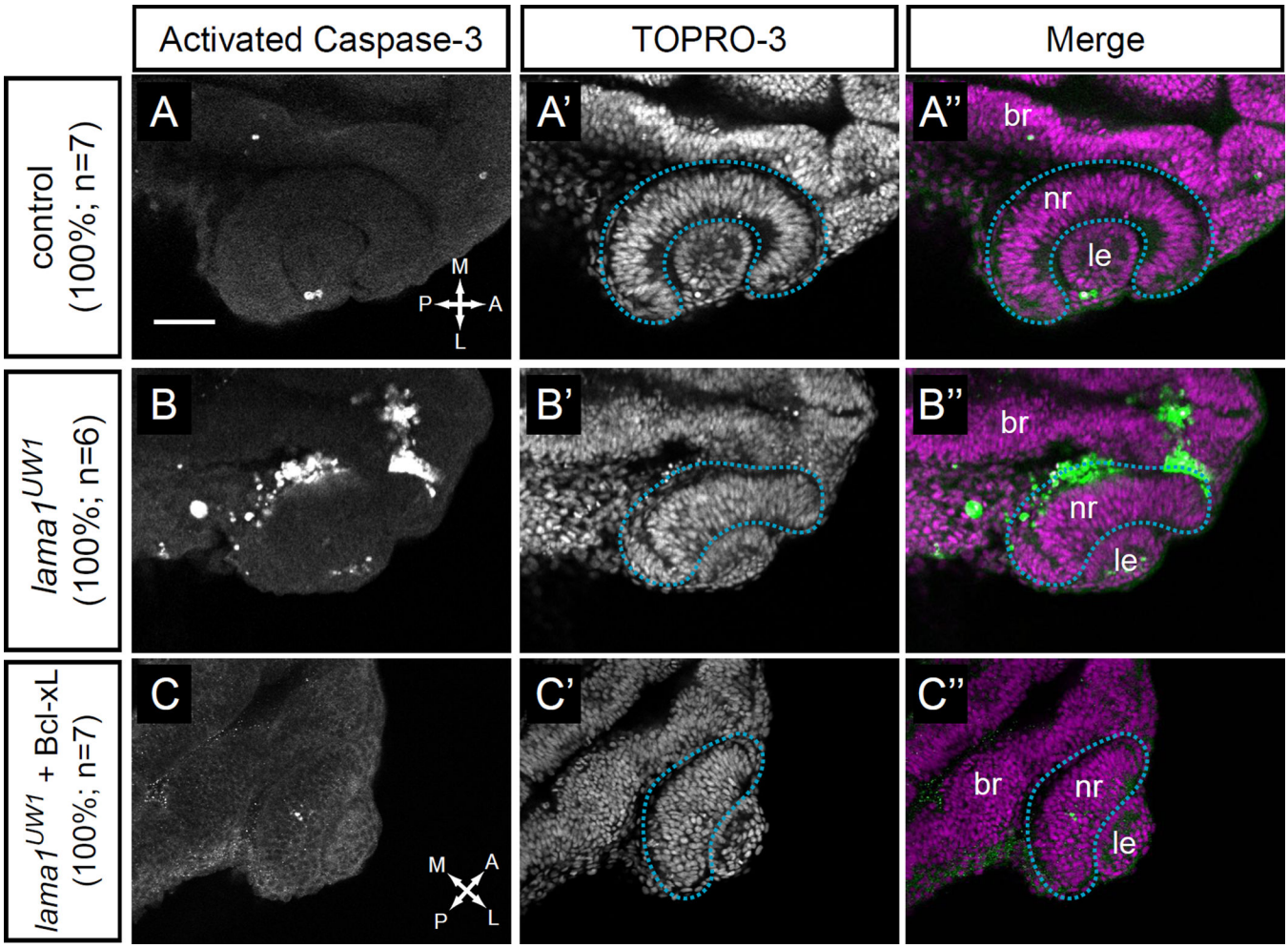

Figure 4.

Apoptosis is increased in *lama1*^{UW1} mutant embryos but is not the underlying cause of morphogenesis defects.

(A-A") Control embryos show little apoptotic cell death. (B-B") *lama1*^{UW1} mutant embryos contain a significant number of dying cells. (C-C") Injection of Bcl-xL RNA (100 pg) rescues apoptosis in *lama1*^{UW1} mutant embryos, however optic cup morphogenesis defects are still apparent.

(A,B,C) Antibody staining for activated caspase-3. (A',B',C') TOPRO-3 counterstain for nuclei. (A", B", C") Merged images. *dashed blue line*, boundary of optic cup. Dorsal views; scale bar, 50 μm. *br*, brain; *nr*, neural retina; *le*, lens. A, anterior; P, posterior; M, medial; L, lateral.

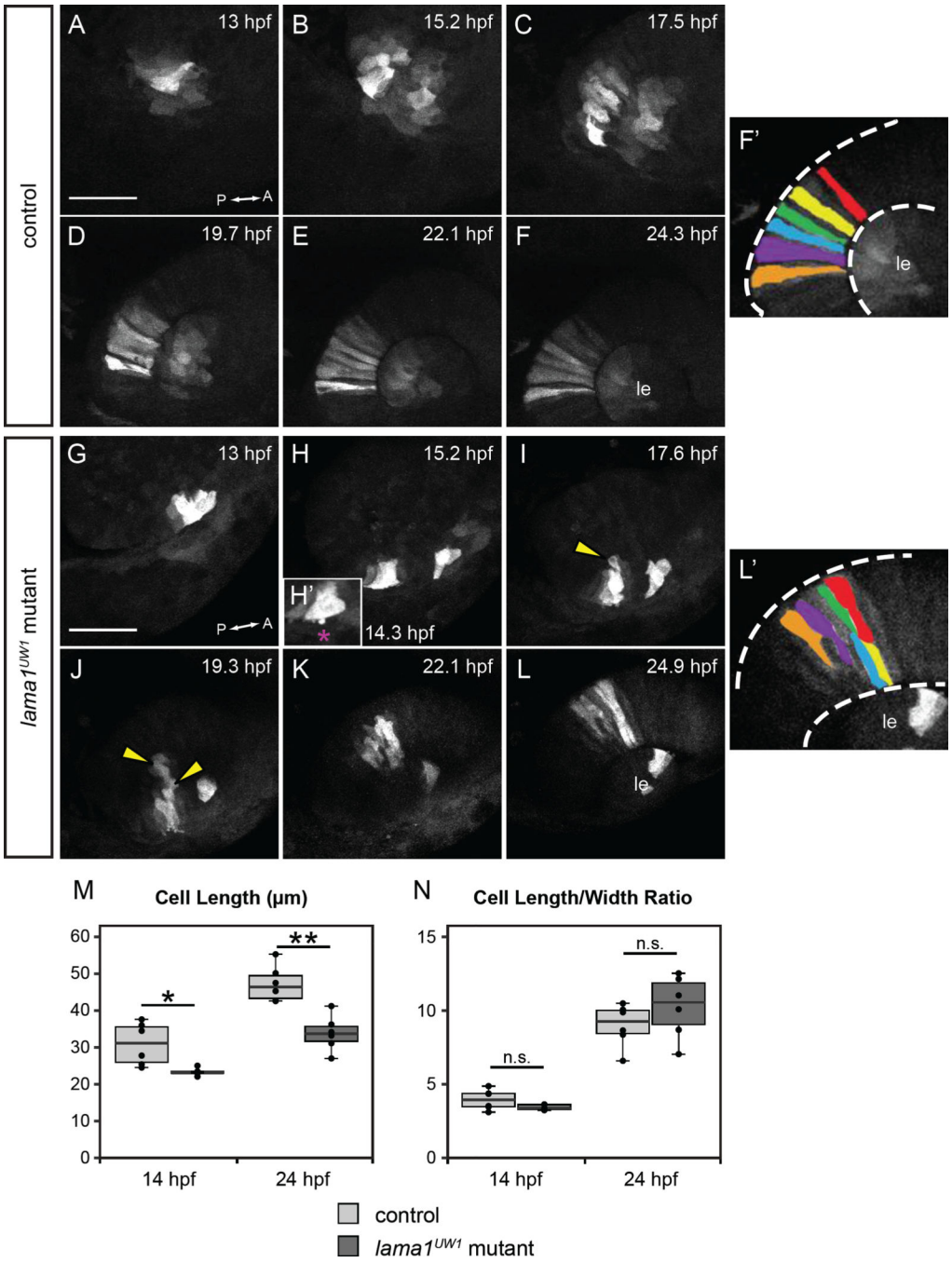

Figure 5.

Loss of motile cell behaviors does not underlie optic cup morphogenesis defects in *lama1*^{UW1} mutant embryos.

Retinal progenitors expressing Kaede were exposed to 405 nm light, which converts Kaede from green to red fluorescence via an irreversible photocleavage. Images are maximum intensity projections from 4-dimensional datasets of the red (converted) channel. (A-F') Images from a timelapse of a *lama1*^{UW1} control sibling embryo. (G-L') Images from a timelapse of a mutant embryo. (H') Zoomed image of single timepoint (14.3 hpf) showing

a retinal progenitor extending a bleb (*magenta asterisk*) beyond the boundary of the optic vesicle. (F', L') Pseudocolor of marked retinal cells. Retinal progenitors in the control embryo extend across the entire width of the retina, while retinal progenitors in the *lama1*^{UW1} mutant embryo elongate, but do not span the width of the retina. Loss of apicobasal register marked by *arrowheads*.

(M, N) Comparisons of length (M) or length/width ratio (N) of retinal progenitors in *lama1*^{UW1} mutant or control embryos. While retinal progenitors are longer in control embryos than mutants, the length/width ratio is not significantly different. *P<0.02; **P<0.001; n.s. = not significant

Dorsal views; scale bar, 50 μm. *le*, lens; dashed lines, retina margins. A, anterior; P, posterior.

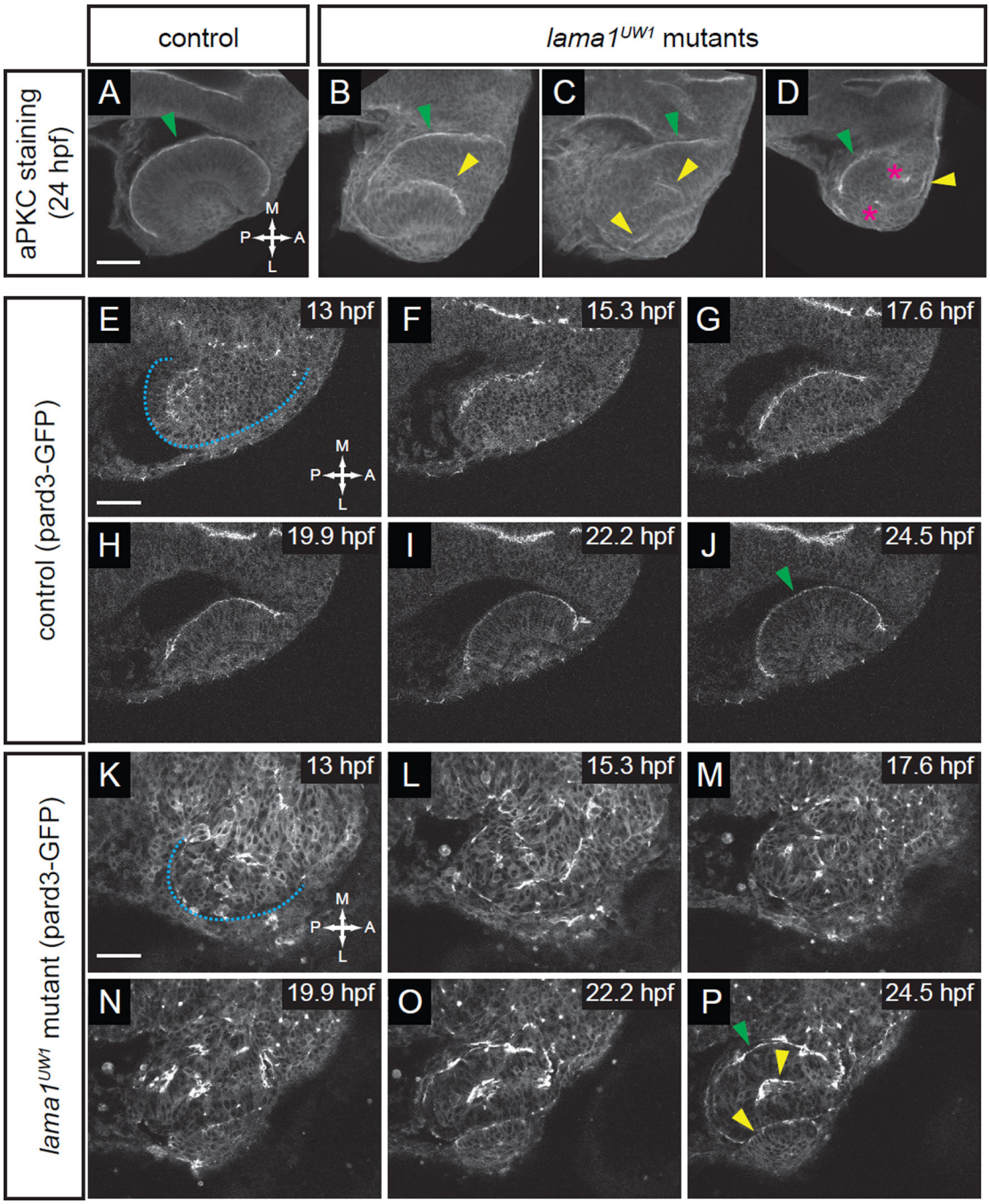

Figure 6.

Apicobasal polarity is disrupted from the earliest stages of optic vesicle morphogenesis. (A–D) Antibody staining for aPKC in control (A) and *lama1*^{UW1} mutant embryos (B–D) reveals disruption of polarity at 24 hpf. *green arrowheads*, correct apical domain. *yellow arrowheads*, ectopic apical domains. *asterisks*, ectopic puncta.

(E–P) Single confocal sections from 4D datasets of apical domain dynamics (marked by pard3-GFP) in a *lama1*^{UW1} control embryo (E–J), or a mutant embryo (K–P). In *lama1*^{UW1} mutant embryos, pard3-GFP localization is disrupted similar to aPKC. *dashed blue line*

marks outline of optic vesicle. *green arrowheads*, correct apical domain. *yellow arrowheads*, ectopic apical domains.

Dorsal views; scale bar, 50 μm. A, anterior; P, posterior; M, medial; L, lateral.

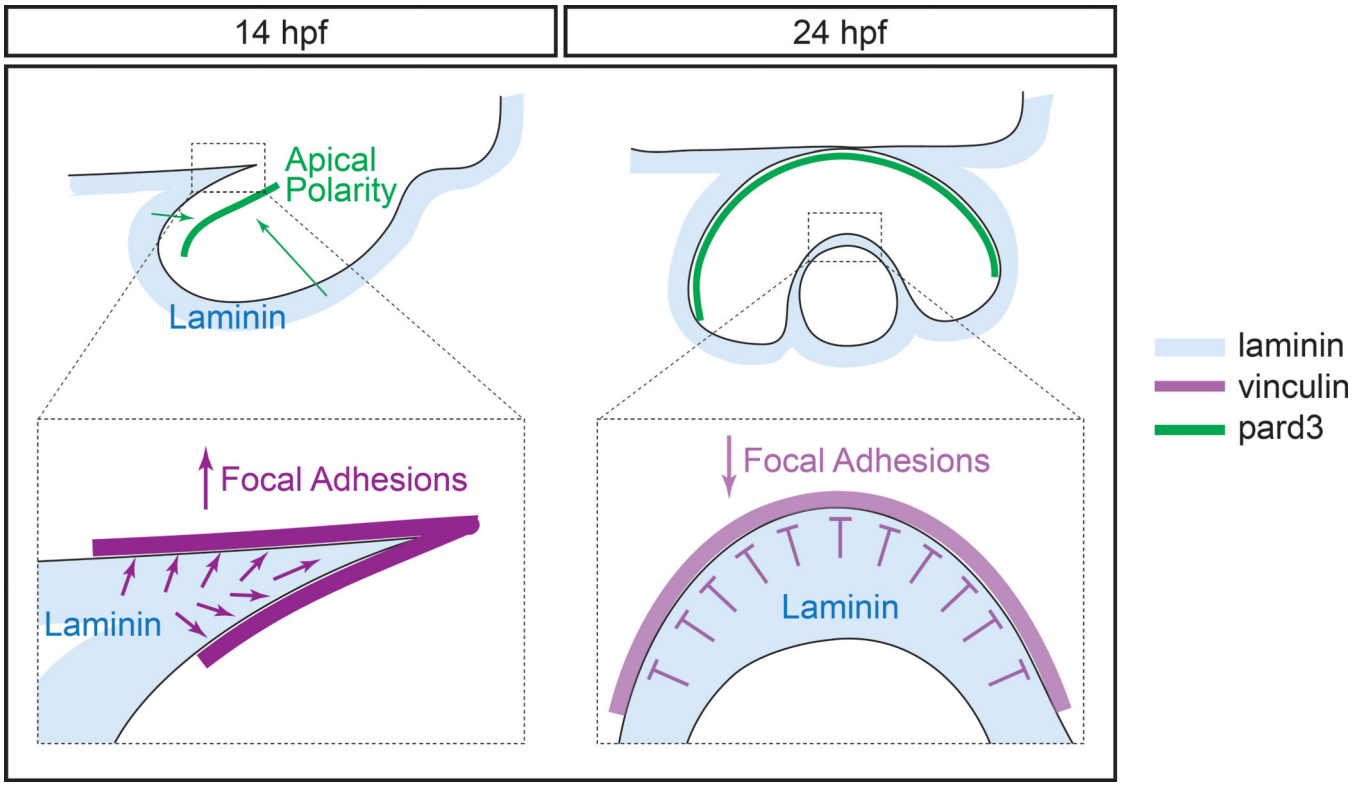

Figure 7.

Model of laminin function during optic vesicle morphogenesis.

During optic vesicle morphogenesis, lama1 is required for establishment of apicobasal polarity, but also has spatiotemporally specific effects on focal adhesions. During optic stalk constriction, lama1 promotes focal adhesion assembly, but during optic cup invagination, lama1 inhibits it.

blue, laminin; *magenta*, vinculin; *green*, pard3.